

## Effect of the Dzyaloshinskii-Moriya interaction on quantum speed limit and orthogonality catastrophe

Zheng-Rong Zhu,<sup>1,2</sup> Qing Wang ,<sup>1</sup> Bin Shao ,<sup>1,2,\*</sup> Jian Zou,<sup>1</sup> and Lian-Ao Wu <sup>3,4,5</sup>

<sup>1</sup>*School of Physics, Beijing Institute of Technology, Beijing 100081, China*

<sup>2</sup>*Yangtze Delta Region Academy of Beijing Institute of Technology, Jiaxing 314019, China*

<sup>3</sup>*Department of Physics, University of the Basque Country UPV/EHU, 48080 Bilbao, Spain*

<sup>4</sup>*IKERBASQUE Basque Foundation for Science, 48013 Bilbao, Spain*

<sup>5</sup>*EHU Quantum Center, University of the Basque Country UPV/EHU, Leioa, Biscay 48940, Spain*



(Received 31 October 2022; accepted 5 April 2023; published 24 April 2023)

We study the effect of the Dzyaloshinskii-Moriya (DM) interaction on the quantum speed limit (QSL) and orthogonality catastrophe (OC) in  $XY$  spin chains. With an initial sudden quench, the general expressions of fidelity and QSL time are derived in terms of the antisymmetric quasiparticle excitation spectra. The numerical and analytical studies show that depending on the system parameters, the DM interaction has various influences on QSL and fidelity. In general, the OC is witnessed and QSL time vanishes in the thermodynamic limit as the variance of the quenched Hamiltonian in ground states scales with the system size, and the conclusion is independent of the DM interaction strength. However, it is interesting to note that the QSL can uniquely detect the critical points and lines induced by the DM interaction. We further analyze the actual evolution speed, a measure of the criticality, and find its direct correspondence with the OC. We also study an interesting phenomenon arising from the magnetic field and DM interaction in the presence of classical noise. Notably, we find that the system dynamic is fault tolerant when the system is subject to a uniform classical noise in the DM interaction strength.

DOI: [10.1103/PhysRevA.107.042427](https://doi.org/10.1103/PhysRevA.107.042427)

### I. INTRODUCTION

The dynamical evolution of a system after a sudden quench is of particular interest in many-body quantum dynamics. One of the significant phenomena in quantum dynamics is the orthogonality catastrophe [1–3] (OC), characterized by the overlap or fidelity between the initial state and the final state. Its importance lies in the sensitivity of many-body systems to external perturbations. It allows one to capture typical features and reveal the physical mechanisms in complicated systems.

Other quantities such as the work distribution [4–6] and quantum speed limit [7–9] (QSL) are also useful in exploring the dynamical properties of many-body systems. In particular, the QSL captures the intrinsic time scaling of a quantum system evolving from an initial state to a target state. It is crucial in various aspects of quantum physics, such as quantum computation [10,11], quantum optimal control [12–14], and quantum metrology [15]. Over the decades, the correlations between the QSL and physical phenomena have been explored, for instance, the interpretation of the geometric measure of entanglement for pure states as the necessary minimal time to separate a given quantum state unitarily [16], potential speedup in a non-Markovian environment [17], a witness of quantum phase transition with QSL [18], and a full characterization of OC by QSL [2,19].

The antisymmetric interaction, Dzyaloshinskii-Moriya (DM) interaction [20,21], often exists in many low-dimensional magnetic materials [22,23] and may induce intriguing phenomena. Interest in the study of the effect of multisite interspin interactions has been rising in the past two decades. Examples include the nonequilibrium steady states with currents [24,25], the adsorption-desorption processes of stochastic kinetics [26], and the Hubbard model higher orders of strong coupling [27]. Moreover, the  $XY$  spin chain [28] provides an excellent foundation to analyze the effect of DM interaction. Phase diagrams of the Ising model and  $XXZ$  model with DM show interesting regions [29]. The dynamical properties of these models were studied in detail [22,30]. Ground-state properties of the spin chain with DM interaction are shown via correlation functions and entanglement [29,31,32]. The effect of the DM interaction on nonequilibrium thermodynamics in the  $XY$  model was analyzed [6]. In addition, the occurrence of dynamical quantum phase transitions (DQPTs) is also affected by the DM interaction [33].

In this paper, we theoretically investigate the effects of the DM interaction on QSL and OC for the  $XY$  spin chain model and pay specific attention to the relation between them. Likewise, we examine the evolution speed which can also characterize the OC. Furthermore, since the occurrence of noise is everywhere without exaggeration, we consider the magnetic field and DM interaction strength with random classical noise.

The paper is organized as follows. In Sec. II, we describe the  $XY$  spin chain system with the DM interaction, and analyze

\*sbin610@bit.edu.cn

the ground-state properties with asymmetrical quasiparticle excitation spectrums. In Sec. III, the theoretic expressions of the QSL time and the fidelity are presented. We then numerically analyze the effects the DM interaction has on QSL and OC. In Sec. IV, we address the behaviors of the evolution speed and relate it to the OC. In Sec. V, we show the influence of the random classical noise. Section VI concludes.

## II. MODELS

The Hamiltonian of the general anisotropic  $XY$  spin chain with DM interaction in the transverse field is given by [6,32,34]

$$H_0 = - \sum_{n=1}^N \left( \frac{1+\gamma}{2} \sigma_n^x \sigma_{n+1}^x + \frac{1-\gamma}{2} \sigma_n^y \sigma_{n+1}^y + h_0 \sigma_n^z \right) - \sum_{n=1}^N D (\sigma_n^x \sigma_{n+1}^y - \sigma_n^y \sigma_{n+1}^x), \quad (1)$$

where  $\sigma_n^{x,y,z}$  are Pauli spin matrices of the  $n$ th site,  $\gamma$  is the anisotropy parameter, and  $h_0$  and  $D$  denote the strength of the external transverse magnetic field and the DM interaction along the  $z$  direction, respectively.

The Hamiltonian (1) can be diagonalized by first employing the standard Jordan-Wigner transformation to map the spins to spinless fermions to

$$H_0 = - \sum_{j=1}^N [(1+2iD)f_j^\dagger f_{j+1} + (1-2iD)f_{j+1}^\dagger f_j + \gamma(f_j^\dagger f_{j+1}^\dagger + f_j f_{j+1}) + h_0(2f_j^\dagger f_j - 1)]. \quad (2)$$

Then we use the Fourier transformation [ $c_k = 1/\sqrt{N} \sum_{j=1}^N f_j e^{-ikj}$ ,  $c_k^\dagger = 1/\sqrt{N} \sum_{j=1}^N f_j^\dagger e^{ikj}$ ,  $k = 2\pi m/N$  with  $m = -(N-1)/2, \dots, (N-1)/2$  for an odd  $N$ ] to convert the Hamiltonian (2) to momentum space and Bogoliubov transformation  $\eta_k = u_k c_k + i v_k c_{-k}^\dagger$  to diagonalize the Hamiltonian as [28]

$$\begin{aligned} H_0 &= \sum_k \varepsilon_k \left( \eta_k^\dagger \eta_k - \frac{1}{2} \right) \\ &= \sum_{k>0} \left[ \varepsilon_k \left( \eta_k^\dagger \eta_k - \frac{1}{2} \right) + \varepsilon_{-k} \left( \eta_{-k}^\dagger \eta_{-k} - \frac{1}{2} \right) \right] \\ &= \sum_{k>0} H_k^0. \end{aligned} \quad (3)$$

Here,  $k$  are the waves vectors, and  $\eta_k$  and  $\eta_k^\dagger$  are the corresponding transformed fermion annihilation and creation operators. The associated  $\varepsilon_k$  are the quasiparticle excitation spectra. Different from general symmetric and positive spectra, in our model with the DM interaction, it can be antisymmetric and negative, and written as [5,6]

$$\varepsilon_k = -4D \sin k + 2\sqrt{(h_0 + \cos k)^2 + \gamma^2 \sin^2 k}. \quad (4)$$

Figure 1 depicts three typical examples of the quasienergy spectra. In light of the properties of the spectra,  $\varepsilon_k$  stay positive for all values of other parameters when  $0 < D \leq \gamma/2$  [35]; see the black solid line in Fig. 1. In this scenario,

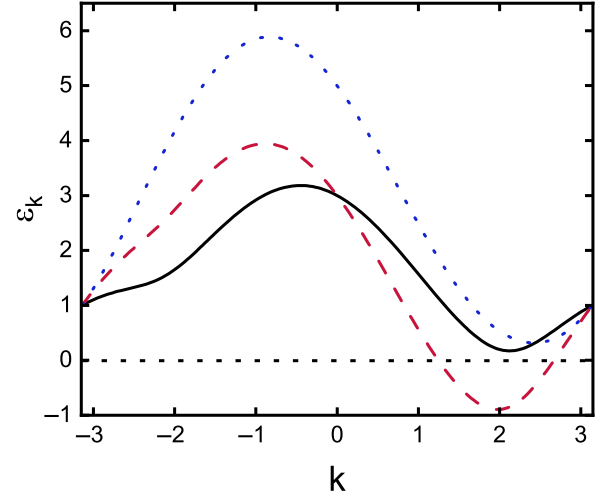


FIG. 1. Three typical quasiparticle energy spectra. The black solid, red dashed and blue dotted lines correspond to  $D = 0.2$ ,  $\gamma = 0.5$ ,  $h_0 = 0.5$ , and  $D = 0.5$ ,  $\gamma = 0.5$ ,  $h_0 = 0.5$ , and  $D = 0.5$ ,  $\gamma = 0.5$ ,  $h_0 = 1.5$ . The black dotted line corresponds to  $\varepsilon_k = 0$ .

the ground state of our model is essentially the vacuum of the Bogoliubov quasiparticles. The ground state is therefore independent of  $D$ , as a consequence of the Bogoliubov transformation not relying on the DM interaction strength. For another case, i.e., the blue dotted line in Fig. 1, where  $h_0^2 > 1 + 4D^2 - \gamma^2$  though  $D > \gamma/2$ , the excitation spectrum stays positive for all  $k$  since the magnetic intensity is dominate. On the other hand, the red dashed line in Fig. 1, for  $D > \gamma/2$  and  $h_0^2 < 1 + 4D^2 - \gamma^2$ , shows that  $\varepsilon_k$  become negative in some ranges of the momentum space. The ground state is now no longer the vacuum of quasiparticles and depends on the value  $D$  for the negative energy in  $k$  space which have to be filled to generate the ground state. In other words, the ground state  $|G\rangle$  of the Hamiltonian corresponds to all states in which  $\varepsilon_k < 0$  and  $\varepsilon_{-k} < 0$  are filled and those with  $\varepsilon_k \geq 0$  and  $\varepsilon_{-k} \geq 0$  are not occupied. The ground state  $|G\rangle$  thus can be written as [36]

$$|G\rangle = \otimes_{k>0} |G\rangle_k, |G\rangle_k = \begin{cases} |0_k 0_{-k}\rangle, \varepsilon_k, \varepsilon_{-k} \geq 0 \\ |0_k 1_{-k}\rangle, \varepsilon_k \geq 0, \varepsilon_{-k} < 0 \\ |1_k 0_{-k}\rangle, \varepsilon_k < 0, \varepsilon_{-k} \geq 0 \\ |1_k 1_{-k}\rangle, \varepsilon_k, \varepsilon_{-k} < 0 \end{cases} \quad (5)$$

As usual,  $|G\rangle_k = |n_k n_{-k}\rangle$ ,  $n_k$  ( $n_{-k}$ ) = 0 or 1 correspond to the eigenvalues of the fermion number operators  $\hat{n}_k = \eta_k^\dagger \eta_k$  ( $\hat{n}_{-k} = \eta_{-k}^\dagger \eta_{-k}$ ).

## III. OC AND QSL

We consider a quantum quench, where the system Hamiltonian  $H_0$  changes to  $\tilde{H}$  with  $h_0$  replaced by  $h_f$  ( $\delta = h_f - h_0$ ). For simplicity, we choose the units where  $\hbar = 1$ . The initial state is prepared in the ground state  $|G\rangle = \otimes_{k>0} |n_k n_{-k}\rangle$ . The ground state of the postquench Hamiltonian  $\tilde{H}$  can be similarly given by  $|\tilde{G}\rangle = \otimes_{k>0} |\tilde{n}_k \tilde{n}_{-k}\rangle$ , where the sign  $\sim$  labels the postquench Hamiltonian and  $\tilde{n}_k$  ( $\tilde{n}_{-k}$ ) are  $\tilde{\eta}_k^\dagger \tilde{\eta}_k$  ( $\tilde{\eta}_{-k}^\dagger \tilde{\eta}_{-k}$ ) accordingly.  $\eta_k$  and  $\tilde{\eta}_k$  are related by the Bogoliubov transformation [5,34,37],  $\tilde{\eta}_k = \cos(\alpha_k) \eta_k -$

$i \sin(\alpha_k) \eta_{-k}^\dagger$ . The relations between eigenstates of  $H_0$  and  $\tilde{H}$  are therefore given by [6,36]

$$\begin{aligned} |0_k 0_{-k}\rangle &= \cos \alpha_k |\tilde{0}_k \tilde{0}_{-k}\rangle + i \sin \alpha_k |\tilde{1}_k \tilde{1}_{-k}\rangle, \\ |1_k 0_{-k}\rangle &= |\tilde{1}_k \tilde{0}_{-k}\rangle, \\ |0_k 1_{-k}\rangle &= |\tilde{0}_k \tilde{1}_{-k}\rangle, \\ |1_k 1_{-k}\rangle &= i \sin \alpha_k |\tilde{0}_k \tilde{0}_{-k}\rangle + \cos \alpha_k |\tilde{1}_k \tilde{1}_{-k}\rangle, \end{aligned} \quad (6)$$

where  $\alpha_k = \tilde{\theta}_k - \theta_k$ , and  $\theta_k$  and  $\tilde{\theta}_k$  are the Bogoliubov angles defined by  $u_k = \cos \theta_k$ ,  $v_k = \sin \theta_k$  and  $\tilde{u}_k = \cos \tilde{\theta}_k$ ,  $\tilde{v}_k = \sin \tilde{\theta}_k$ . In our model, the angles  $\theta_k = 1/2 \arctan[\gamma \sin k / (h_0 + \cos k)]$ ,  $\tilde{\theta}_k = 1/2 \arctan[\gamma \sin k / (h_f + \cos k)]$  [34] and they are independent of  $D$ .

The fidelity  $F(t)$ , a vital quantity in the OC, is defined as a dynamical overlap between the initial state and final state evolving from pre- and postquench Hamiltonians. This is closely related to the Loschmidt echo [38–40] (LE) and formulated as

$$\begin{aligned} F(t) &= |\langle G | e^{i\tilde{H}t} e^{-iH_0 t} | G \rangle|^2, \\ F(t) &= \otimes_{k>0} |F_k(t)|^2. \end{aligned} \quad (7)$$

Then, using Eqs. (3), (5), and (6), one obtains [36]

$$F_k(t) = \begin{cases} \cos^2 \alpha_k + \sin^2 \alpha_k e^{-it(\tilde{\varepsilon}_k + \tilde{\varepsilon}_{-k})}, & \varepsilon_k, \varepsilon_{-k} \geq 0 \\ e^{-it(\tilde{\varepsilon}_k + \tilde{\varepsilon}_{-k})}, & \varepsilon_k \geq 0, \varepsilon_{-k} < 0 \\ e^{-it(\tilde{\varepsilon}_k + \tilde{\varepsilon}_{-k})}, & \varepsilon_k < 0, \varepsilon_{-k} \geq 0 \\ \sin^2 \alpha_k + \cos^2 \alpha_k e^{-it(\tilde{\varepsilon}_k + \tilde{\varepsilon}_{-k})}. & \varepsilon_k, \varepsilon_{-k} < 0 \end{cases} \quad (8)$$

The QSL time is directly connected with the fidelity by [2,8,19]

$$\tau \geq \tau_{\text{QSL}} = \frac{\arccos \sqrt{F(t)}}{\Delta H_f}. \quad (9)$$

The variance of the postquench Hamiltonian  $\Delta H_f$ , regarded as the maximal rate of quantum evolution  $v_{\text{QSL}}$ , is given by  $\Delta H_f = \sqrt{\sum_{k>0} \Delta H_{k,f}^2}$  [8,19], where

$$\Delta H_{k,f}^2 = \begin{cases} \sin^2 2\alpha_k \left(\frac{\tilde{\varepsilon}_k + \tilde{\varepsilon}_{-k}}{2}\right)^2, & \varepsilon_k \cdot \varepsilon_{-k} \geq 0 \\ 0, & \varepsilon_k \cdot \varepsilon_{-k} \leq 0 \end{cases} \quad (10)$$

Now we begin to show the effects of the DM interaction on the QSL and OC. Figure 2 depicts the QSL time  $\tau_{\text{QSL}}$  and the fidelity  $F$  as functions of  $t$  for different strengths of the DM interaction. It clearly shows that when  $D \leq \gamma/2$ , both  $\tau_{\text{QSL}}$  and  $F$  are insensitive to  $D$  [35,41] because the ground state of the initial Hamiltonian is independent of  $D$ . However, for  $D > \gamma/2$ , a slight change of the DM interaction strength would lead to different behaviors. The QSL time and the fidelity then show oscillations over time. The numerical results also imply that the larger the DM strength is, the higher oscillation frequency the QSL time and fidelity are. In addition, the decay of the fidelity is suppressed with  $D$ , while QSL time oscillates around a smaller value in long-time evolution. To summarize, when  $D$  is large and the oscillation frequency increases and decay amplitude decreases, the DM interaction dominates the system. This is because some momentum space

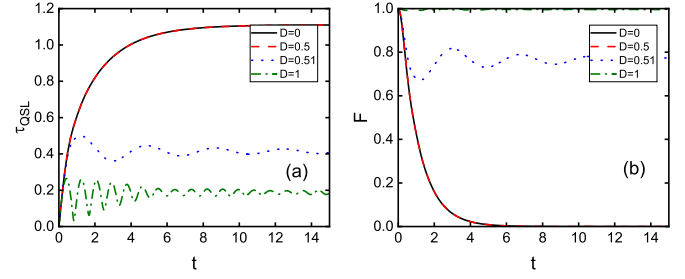


FIG. 2. (a) QSL time  $\tau_{\text{QSL}}$  and (b) fidelity  $F$  as functions of time  $t$  for different values of  $D$ . The parameters are  $N = 801$ ,  $h_0 = 1$ ,  $\gamma = 1$ , and  $\delta = 0.05$ .

modes in  $F_k(t)$  in Eq. (8), determined by system parameters, do not contribute and remain unity, and  $\Delta H_{k,f}^2$  in Eq. (10) for a range of  $\varepsilon_k \cdot \varepsilon_{-k} \leq 0$  are zeros.

The dependence on initial magnetic intensity, as shown in Fig. 3, is of interest. There are two notable features. First, it shows a parallel insensitivity to  $D$  for  $D < \gamma/2$ , regardless of the magnetic intensity. And a particular transformation from peaked  $\tau_{\text{QSL}}$  to a sharp valley at  $h_0 = 1$  can be observed, while the fidelity behaves the opposite. Moreover, this is a significant indication of a quantum phase transition, i.e., a transition from a ferromagnetic phase to chiral phase induced by DM interaction [41]. Second, when  $h_0 \geq 1$ , we show that the turning points marked by circles exhibit interesting behaviors, as in Fig. 4. A good agreement between the numerical and theoretic results can be clearly seen. It is interesting to note that the QSL time can signal the critical points and lines of the quantum phase transitions.

Next, we shed light on the influence of the DM interaction for anisotropy parameters  $\gamma \in (0, 1)$ . In Fig. 5,  $\tau_{\text{QSL}}$  shows an enhanced decay for  $\gamma \in (0, 2D)$  in comparison with the cases without the DM interaction (black solid line), while  $F$  decrease in this scenario. The critical points  $\gamma = 2D$  are clearly seen, while for  $D > 0.5$ , the chiral phase region expands and all the  $\gamma \in (0, 1)$  at  $h_0 = 1$  are in this region. Thus, a slight quench difference  $\delta = 0.05$  causes trivial dynamics and we can see that  $F$  keeps close to unity and  $\tau_{\text{QSL}}$  is small for  $\gamma \in (0, 1)$ . Further, we examine the QSL time and the fidelity versus  $D$ , with different initial conditions for  $h_0$  and  $\gamma$ . Figure 6(b) shows that the large enough DM interaction can suppress the decay of fidelity, while the QSL time is more complicated to some extent. To illustrate, when  $D < \gamma/2$ , both  $\tau_{\text{QSL}}$  and  $F$  are not sensitive to the DM interaction. On the other hand, when  $h_0 > 1$ ,  $\tau_{\text{QSL}}$  and  $F$  are not influenced by the DM interaction until it reaches the critical  $D_c = \frac{1}{2} \sqrt{h_0^2 + \gamma^2} - 1$ . This may be attributed to the pre- and postquench systems with a small quench difference  $\delta$  being in the paramagnetic phase, where the magnetic intensity dominates. When the DM interaction is out of the critical  $D_c$ ,  $\tau_{\text{QSL}}$  is determined by the trade-off between the fidelity and the variance of the postquench Hamiltonian. It can be clearly seen that from a comparison between the black solid and red dashed lines in Figs. 6(b) and 6(c), although they show the same behaviors in variance, a difference in  $h_0$  makes a big change in the  $\tau_{\text{QSL}}$ . Similar behaviors of the  $\tau_{\text{QSL}}$ , which is determined by the competition between the variance and

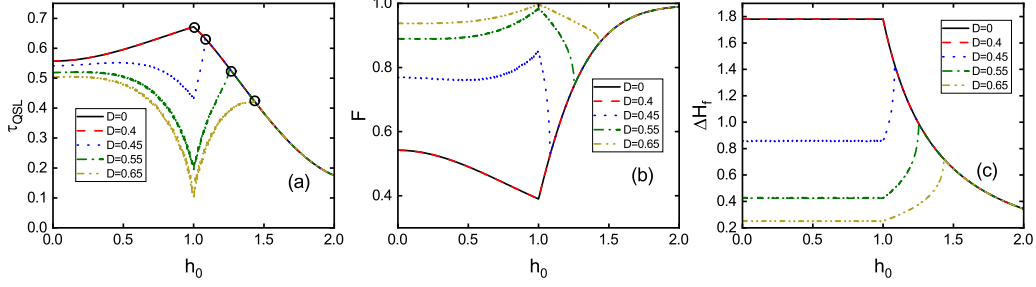


FIG. 3. Dependence on  $h_0$  for an increase of  $D$  with other parameters:  $N = 801$ ,  $\gamma = 0.8$ ,  $t = 1$ , and  $\delta = 0.05$ . (a)  $\tau_{\text{QSL}}$ , (b)  $F$ , and (c)  $\Delta H_f$ .

the fidelity, are witnessed; if we keep the same  $h_0 = 1$ ,  $\gamma$  varies from 0.8 to 0.4. Therefore,  $\tau_{\text{QSL}}$  behaves in a more complicated way as for the different  $h_0$  and  $\gamma$  parameters.

Finally, we plot the QSL time and fidelity as functions of the system size under different DM interactions, depicted in Fig. 7. For smaller  $D$ , the fidelity vanishes when the system size increases and can be a witness of the OC. When  $D = 0.75$ , the fidelity does not decay to zero with the system size, even in a magnitude of  $10^5$ . It means more spins are required for the fidelity to vanish, and larger DM interaction can greatly suppress the decay of the fidelity. Also, we have done the curve fitting of the fidelity decay and it is exponential  $e^{-N/t_1}$ , where  $t_1$  is the fitting exponent. The exponents extracted from our data are 2056.2, 9454.9, and 233 327 for DM strength  $D = 0.51$ ,  $D = 0.55$ , and  $D = 0.75$ , respectively, while for  $D = 0$  and  $D = 0.5$ , they have the same exponent, 936.78. Meanwhile, the QSL time decays with  $N$  for all DM interaction strengths. The variance, as shown in Fig. 7(c), scales with  $N$ , but is a decrease function of  $D$  when  $D > \gamma/2$ . In this case, the larger  $D$  is, the slower  $\tau_{\text{QSL}}$  decays with system size. As a last remark, the complexity of the QSL time, as mentioned before, can be seen as a result of the trade-off between the variance and the fidelity.

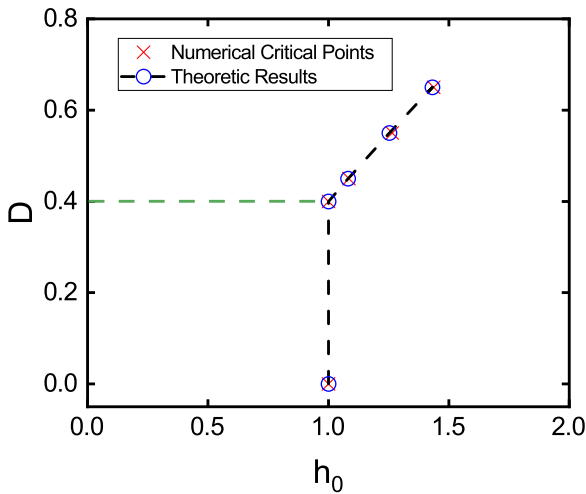


FIG. 4. The location of turning points in the  $D$ - $h_0$  plane with the same configurations as in Fig. 3. The black dashed line denotes the critical point  $h_c = 1$  for  $D < \gamma/2$  and the critical line  $h_c = \sqrt{1 + 4D^2 - \gamma^2}$  for  $D > \gamma/2$ . The green dashed line corresponds to  $D = \gamma/2$ .

#### IV. PRACTICAL EVOLUTION SPEED

In this section, we will study the effect of the DM interaction on the evolution speed of the impurity qubit since it is closely related to the OC [42]. The speed of the corresponding evolution is termed by resorting to Riemannian metric  $\mathbf{g}$  defined on the space of the quantum state [8,43,44]. By adopting the quantum Fisher information metric [45], we can define the speed of the quantum evolution at time  $t$  by deriving the distance between neighboring states,

$$v(t) = \frac{ds}{dt} = \sqrt{g(t)} \quad (11)$$

and

$$g(t) = -2 \frac{d^2}{dt^2} F(\rho(0), \rho(t)), \quad (12)$$

where  $F(\rho(0), \rho(t)) = (\text{Tr}\{[\sqrt{\rho(0)}\rho(t)\sqrt{\rho(0)}]^{1/2}\})^2$  is the Uhlmann fidelity between the initial state  $\rho(0)$  and final state  $\rho(t)$  of the impurity.

The impurity qubit interacts with the XY spin chain bath through  $H_I = -\frac{\delta}{2}|e\rangle\langle e| \sum_{n=1}^N \sigma_n^z$ . We initialize the single qubit in a superposition state  $|\psi\rangle = c_g|g\rangle + c_e|e\rangle$ , where  $c_g^2 + c_e^2 = 1$ . The spin chain state is prepared in the ground state  $|G\rangle$  and assume the impurity qubit is not correlated with the spin chain bath. The dynamic of the impurity qubit is a typical decoherence process characterized by the decoherence factor  $f(t) = \otimes_{k>0} F_k(t)$ , where its norm is the aforementioned fidelity. Let us assume  $c_g = \cos \frac{\theta}{2}$ ,  $c_e = e^{i\phi} \sin \frac{\theta}{2}$ ; then the Bloch vector of the two-level qubit system is given by

$$\vec{n}(0) = \{\sin \theta \cos \phi, \sin \theta \sin \phi, \cos \theta\}, \quad (13)$$

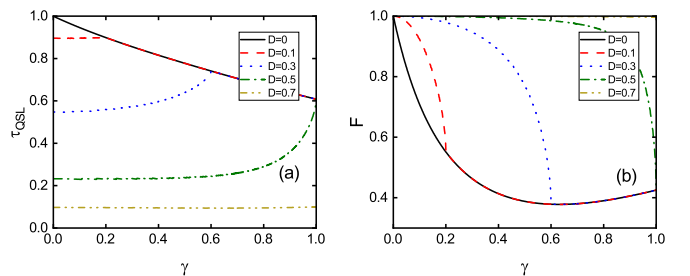


FIG. 5. (a)  $\tau_{\text{QSL}}$  and (b)  $F$  as functions of  $\gamma$ . Different DM interaction values are investigated. Here, we fix evolution time  $t = 1$ , magnetic intensity  $h_0 = 1$ , system size  $N = 801$ , and quench difference  $\delta = 0.05$ .

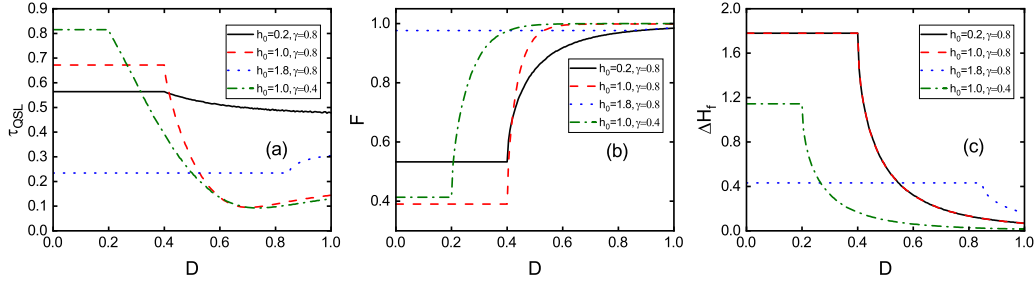


FIG. 6. (a)  $\tau_{\text{QSL}}$ , (b)  $F$ , and (c)  $\Delta H_f$  vs  $D$  with different choices of magnetic intensity and anisotropy parameters. Other parameters:  $N = 801$ ,  $\tau = 1$ , and  $\delta = 0.05$ .

where  $\theta \in [0, \pi]$  and  $\phi \in [0, 2\pi]$ . The fidelity between  $\rho(0)$  and  $\rho(t)$  can be obtained by

$$F(\rho(0), \rho(t)) = \frac{1}{2} \{1 + \bar{n}(0) \cdot \bar{n}(t) + \sqrt{[1 - \bar{n}(0) \cdot \bar{n}(0)][1 - \bar{n}(t) \cdot \bar{n}(t)]}\}, \quad (14)$$

where the Bloch vector  $\bar{n}(t)$  accounts for the decoherence factor of the evolved state  $\rho(t)$ . Therefore, the evolution speed can be obtained via the above general formula of a two-level quantum system as [45,46]

$$v(t) = \sqrt{|\text{Re}[\ddot{f}(t) \sin^2 \theta]|}, \quad (15)$$

where we assume  $\theta = \frac{\pi}{2}$ ,  $\phi$  can be any values in the range  $[0, 2\pi]$ . We relate it to the OC and calculate the time-averaged evolution speed,

$$V_{\text{average}} = \frac{1}{t_D} \int_0^{t_D} v(t) dt, \quad (16)$$

where  $t_D$  is the driving time. We now look into the quantum speed limit  $V_{\text{qsl}}$  of the qubit to show its relation to the evolution speed. Using the Bures angle,  $L(\rho(0), \rho(t)) = \arccos \sqrt{\langle \psi | \rho(t) | \psi \rangle}$  between the initial pure state  $\rho(0) = |\psi\rangle\langle\psi|$  and final evolved state  $\rho(t)$ . The dynamic evolution of the qubit density matrix  $\rho(t)$  is known. Then, after some simple algebra, the exact form of the  $V_{\text{qsl}}$  can be written as

$$V_{\text{qsl}} = \frac{1}{t_D} \int_0^{t_D} |\partial_t f(t)| dt. \quad (17)$$

This quantum speed limit  $V_{\text{qsl}}$  of the qubit is characterized by the Margois-Levitin (ML)-type bound which is based on the operator norm.

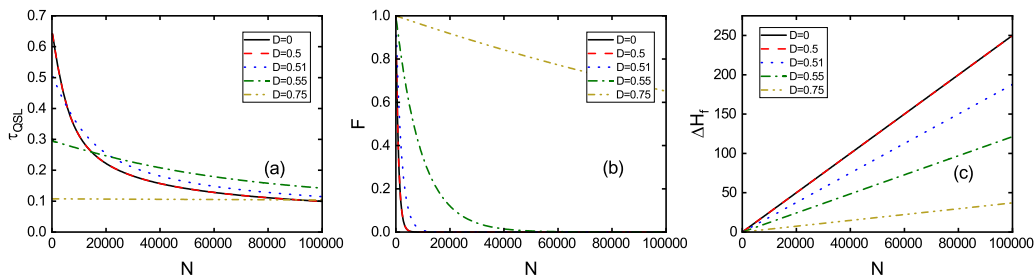


FIG. 7. (a)  $\tau_{\text{QSL}}$  and (b)  $F$  as functions of  $N$  at different DM interaction values. The other parameters are set as  $h_0 = 1$ ,  $\gamma = 1$ ,  $t = 1$ , and  $\delta = 0.05$ .

In Fig. 8, we plot them as a function of the initial magnetic field. It is easy to find that the two quantities exhibit similar behaviors, while they are calculated from different physical concepts. Alternatively, there exists a sudden change at  $h_0 = 1$  when the DM interaction  $D \leq \gamma/2$ ; see the insets for a clearer description of the discontinuity, indicating a quantum phase transition. In addition, when  $D > \gamma/2$ , the critical points of system  $h_c = \sqrt{1 + 4D^2 - \gamma^2}$  appear. Therefore, it is interesting that the actual evolution speed and the quantum speed limit can also reveal the criticality of the system.

To comprehend the relation between the evolution speed and OC, Fig. 9 shows the time-averaged evolution speed and the quantum speed limit as a function of  $N$ . The inset is the case of  $D = 0$ , which grows slowly with  $N$ . It shows that they both grow linearly with size, which is the same as the variance  $\Delta H_f$ , and hence we can also conclude that the evolution speed can characterize the OC.

## V. NOISE EFFECT

Now we consider the magnetic intensity with random classical noise  $\alpha$  from various sources, for example, disturbances in Earth's magnetic field. When the system initially is in the ground state  $|G\rangle$  of the Hamiltonian  $H_0$ , the evolving density matrix  $\rho(t)$  can be expressed as

$$\rho(t) = \frac{\sum_{\alpha} e^{-iH_f^{\alpha} t} |G\rangle\langle G| e^{iH_f^{\alpha} t}}{\text{tr}(\sum_{\alpha} e^{-iH_f^{\alpha} t} |G\rangle\langle G| e^{iH_f^{\alpha} t})}, \quad (18)$$

where  $H_f^{\alpha}$  is the quenched Hamiltonian with noise. The fidelity follows the standard definition for mixed states,

$$F(t) = \langle \psi(t) | \rho(t) | \psi(t) \rangle, \quad (19)$$

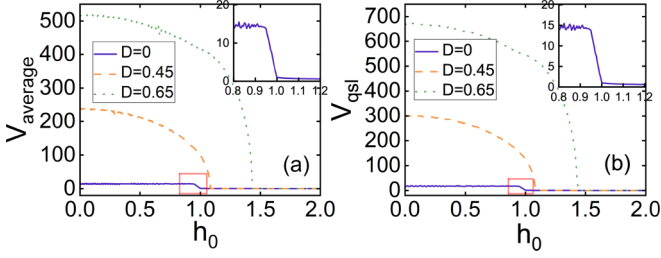


FIG. 8. (a) The time-averaged evolution speed  $v_{\text{average}}$  and (b) the quantum speed limit  $V_{\text{qsl}}$  as a function of magnetic intensity  $h_0$  for different values of  $D$ . Related parameters are  $N = 801$ ,  $t_D = 1$ ,  $\gamma = 0.8$ , and  $\delta = 0.05$ .

where  $|\psi(t)\rangle = e^{-iH_0 t}|G\rangle$ , and the Hamiltonian  $H_0$  is exactly the initial unperturbed Hamiltonian. By introducing the evolving density matrix (18) into Eq. (19), we get

$$F(t) = \frac{\sum_{\alpha} \langle G|e^{iH_0 t} e^{-iH_f^{\alpha} t}|G\rangle \langle G|e^{iH_f^{\alpha} t} e^{-iH_0 t}|G\rangle}{\text{tr}(\sum_{\alpha} e^{-iH_f^{\alpha} t}|G\rangle \langle G|e^{iH_f^{\alpha} t})}, \quad (20)$$

where the denominator can be straightforwardly calculated.

The minimum time for the initial state to evolve to the final state is defined as the QSL time. It can be obtained by seeing noises acting as many quantum channels and using the bound derived in Ref. [47]. Note that the initial state is taken as a pure state and  $\text{tr}\{\rho_0^2\} = 1$ . Then, after simple derivations, the QSL time with noise can be written as

$$\tau_{\text{QSL}} \geq \frac{2(\arccos F)^2}{\pi^2} \frac{1}{\sum_{\alpha} \|K_{\alpha} \rho_0 K_{\alpha}^{\dagger}\|}, \quad (21)$$

where  $\bar{X} = t^{-1} \int_0^t X dt$ ,  $\|A\| = \sqrt{\text{tr}(A^{\dagger} A)}$  is the Hilbert-Schmidt norm of the operator  $A$ , and  $K_{\alpha} = 1/\sqrt{M} \exp[-i(H_f^{\alpha} - \langle G|H_f^{\alpha}|G\rangle)t]$ . Hence we get

$$\sum_{\alpha} \|K_{\alpha} \rho_0 K_{\alpha}^{\dagger}\| = \frac{1}{M} \sum_{\alpha} \Delta H_f^{\alpha}, \quad (22)$$

where  $\Delta H_f^{\alpha}$  is the variance of the quenched Hamiltonian with noise and  $M$  is the specific number of magnetic noise  $\alpha$ .

Noise could happen in all dynamical processes, for example, modeled with a DM strength disturbed by noise  $\beta$ . Then the time-evolving density matrix  $\rho(t)$  can be written as

$$\rho(t) = \frac{\sum_{\beta} e^{-iH_f^{\beta} t}|G\rangle \langle G|e^{iH_f^{\beta} t}}{\text{tr}(\sum_{\beta} e^{-iH_f^{\beta} t}|G\rangle \langle G|e^{iH_f^{\beta} t})}. \quad (23)$$

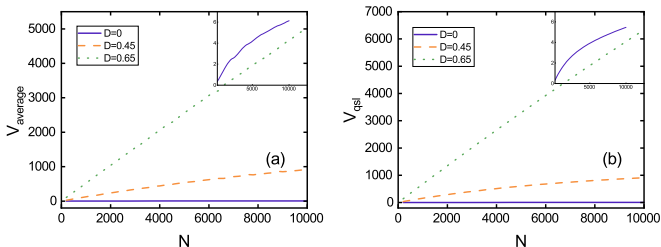


FIG. 9. (a)  $V_{\text{average}}$  and (b)  $V_{\text{qsl}}$  vs  $N$  for different DM strengths. Other parameters:  $h_0 = 1$ ,  $\delta = 0.05$ ,  $\gamma = 0.8$ , and  $t_D = 1$ .

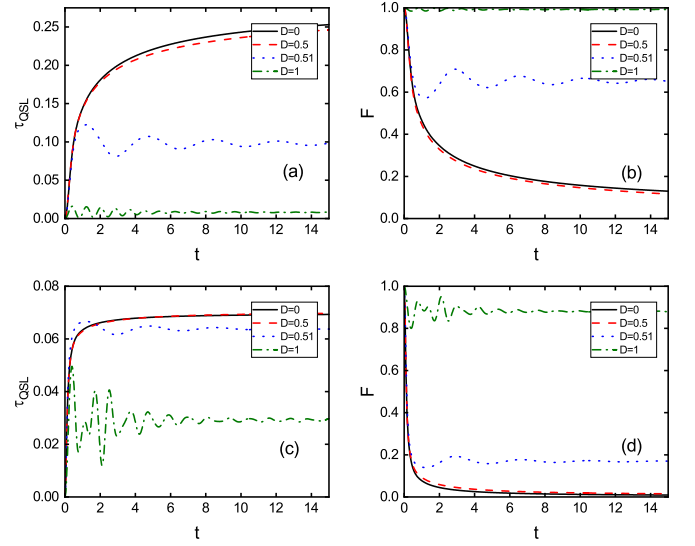


FIG. 10. (a)  $\tau_{\text{QSL}}$  and (b)  $F$  vs  $t$  for different DM strengths, with the noise  $\alpha \in (-0.1h_0, 0.1h_0)$ . (c)  $\tau_{\text{QSL}}$  and (d)  $F$  vs  $t$  for different DM strengths, with the noise  $\alpha \in (-0.5h_0, 0.5h_0)$ . Other parameters:  $h_0 = 1$ ,  $h_f = 1.05$ ,  $\gamma = 1$ ,  $M = 500$ , and  $N = 801$ .

The fidelity becomes

$$F(t) = \frac{\sum_{\beta} \langle G|e^{iH_0 t} e^{-iH_f^{\beta} t}|G\rangle \langle G|e^{iH_f^{\beta} t} e^{-iH_0 t}|G\rangle}{\text{tr}(\sum_{\beta} e^{-iH_f^{\beta} t}|G\rangle \langle G|e^{iH_f^{\beta} t})}, \quad (24)$$

where  $H_f^{\beta}$  is the quenched Hamiltonian with DM noise  $\beta$ . Following the same procedure in tackling the magnetic noise, and according to the Eqs. (4), (7), and (8), the DM noise term does not affect the fidelity since  $\alpha_k$  and  $\tilde{\varepsilon}_k + \tilde{\varepsilon}_{-k}$  are independent of  $\beta$ . In other words, the QSL time and fidelity are fault tolerant against noise due to the DM strength.

In what follows, the system dynamics under the effects of magnetic noise  $\alpha$  are numerically shown in Fig. 10, where we illustrate for noise in the intervals, i.e.,  $\alpha \in (-0.1h_0, 0.1h_0)$  and  $\alpha \in (-0.5h_0, 0.5h_0)$ , and other system parameters are the same as the case without noise in Fig. 2. In contrast to the noiseless case, the first observation is that a minor difference is witnessed between  $D = 0$  and  $D = 0.5$ , which is induced by the randomness of the noise. While it is believed that as the number of noise  $M \rightarrow \infty$ , both coalesce to one due to the averaging effect. Another discrepancy is that the QSL times stay or oscillate around a smaller value in the noise case, which means that the intrinsic minimum decreases with noise. Furthermore, the fidelity, under the effects of noise, display different behaviors for  $D \leq \gamma/2$  and  $D > \gamma/2$ , i.e., the fidelity with  $D \leq \gamma/2$  is suppressed, and with  $D > \gamma/2$ , it is enhanced.

For an investigation of the OC phenomenon, we examine the dynamic behaviors of the QSL and fidelity with the DM strength set as  $D = 0.51$ , and different system sizes  $N = \{801, 5001, 10001, 20001\}$ , in Fig. 11. The imposed noise is in the regimes mentioned above. It is clearly seen that the fidelity decays more sharply as  $N$  increases and the stable value after a short time decays smaller. This is also witnessed by a lower oscillation center of the QSL time presenting a

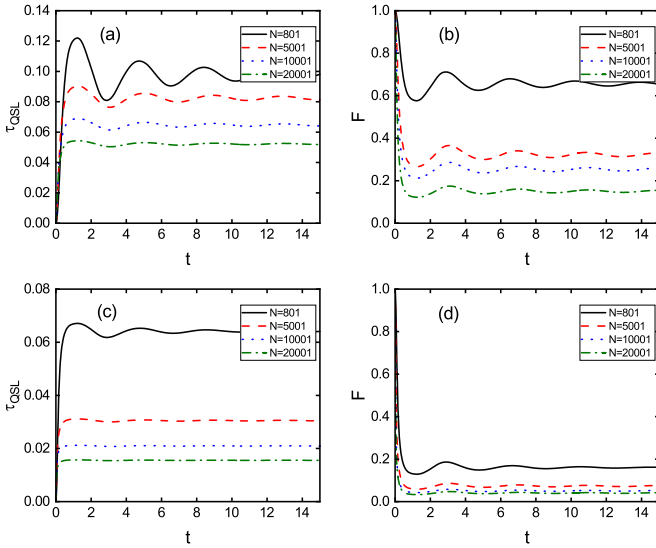


FIG. 11. (a)  $\tau_{\text{QSL}}$  and (b)  $F$  vs  $t$  for  $N = \{801, 5001, 10001, 20001\}$ , with the noise  $\alpha \in (-0.1h_0, 0.1h_0)$ . (c)  $\tau_{\text{QSL}}$  and (d)  $F$  vs  $t$ , with the noise  $\alpha \in (-0.5h_0, 0.5h_0)$ . Other parameters:  $h_0 = 1$ ,  $h_f = 1.05$ ,  $\gamma = 1$ ,  $M = 500$ , and  $D = 0.51$ .

signature of the OC, and the effect of noise naturally arises if comparing it with the noiseless case. In addition, the system dynamic with noise in a broader variation range is greatly enhanced.

## VI. CONCLUSIONS

In this work, we have analyzed the effects of the DM interaction on QSL and the fidelity as a vital quantity in the OC. Our results show that the QSL time and fidelity are insensitive to the DM interaction when  $D \leq \gamma/2$  for arbitrary  $h_0$  and  $D < \frac{1}{2}\sqrt{h_0^2 + \gamma^2} - 1$  for  $h_0 > 1$ . The former case originates from the initial ground state being the vacuum of Bogoliubov quasiparticles independent of the DM interaction when  $D \leq \gamma/2$ . And in the latter case in which  $h_0 > 1$  and

$D < \frac{1}{2}\sqrt{h_0^2 + \gamma^2} - 1$ , the pre- and postquenches are in the same paramagnetic phase where the magnetic field dominates and  $\varepsilon_k$  is positive for all  $k$  modes. Hence the DM interaction does not have influence on the QSL time and fidelity. The impacts of the DM interaction emerge when  $D$  is beyond the critical points, and it has a complicated influence on the QSL time due to a trade-off between the fidelity and variance of the postquench Hamiltonian in the initial ground states. The QSL time will vanish in the thermodynamic limit as a scaling with system size. We see that the DM interaction plays the role of suppressing the decay of the fidelity, and the larger the DM interaction strength is, the more spins are needed for the witness of the OC. It is also interesting to note that the QSL time is a useful tool to indicate the quantum phase transition and identify the critical points and lines induced by the DM interaction.

We also examined the behaviors of the actual evolution speed of the impurity qubit. It shows that the evolution speed scales as  $N$ , which can be seen as a characterization of the OC. And we have revealed a similar behavior that the actual speed and the quantum speed limit of the qubit share. As such, it is worth noting that the formalism of the actual evolution speed provides a valuable framework to explore the properties of the given dynamics as the QSL does. In addition, we have explored the role of noise in the dynamics of the quantum many-body system. The QSL time under the magnetic noise effect is suppressed, while the fidelity show considerably different behaviors for the two regions  $D \leq \gamma/2$  and  $D > \gamma/2$ . Interestingly, we find that the QSL time and fidelity are fault tolerant against the DM noise.

## ACKNOWLEDGMENTS

We gratefully acknowledge support from the National Natural Science Foundation of China under Grants No. 11875086 and No. 11775019. L.-A.W. is supported by the Basque Country Government (Grant No. IT1470-22) and Grant No. PGC2018-101355-B-I00 funded by MCIN/AEI/10.13039/501100011033.

- [1] P. W. Anderson, *Phys. Rev. Lett.* **18**, 1049 (1967).
- [2] T. Fogarty, S. Deffner, T. Busch, and S. Campbell, *Phys. Rev. Lett.* **124**, 110601 (2020).
- [3] J. Goold, T. Fogarty, N. Lo Gullo, M. Paternostro, and T. Busch, *Phys. Rev. A* **84**, 063632 (2011).
- [4] A. Silva, *Phys. Rev. Lett.* **101**, 120603 (2008).
- [5] M. Zhong and P. Tong, *Phys. Rev. E* **91**, 032137 (2015).
- [6] Q. Wang, D. Cao, and H. T. Quan, *Phys. Rev. E* **98**, 022107 (2018).
- [7] S. Deffner and S. Campbell, *J. Phys. A: Math. Theor.* **50**, 453001 (2017).
- [8] M. M. Taddei, B. M. Escher, L. Davidovich, and R. L. de Matos Filho, *Phys. Rev. Lett.* **110**, 050402 (2013).
- [9] W. K. Wootters, *Phys. Rev. D* **23**, 357 (1981).
- [10] N. Margolus and L. B. Levitin, *Physica D* **120**, 188 (1998).
- [11] H. J. Bremermann, in *Proceedings of the Fifth Berkeley Symposium on Mathematical Statistics and Probability*, edited by L. M. Le Cam and J. Neyman (University of California Press, Berkeley, CA, 1967), Vol. 4, pp. 15–20.
- [12] P. Pfeifer, *Phys. Rev. Lett.* **70**, 3365 (1993).
- [13] T. Caneva, M. Murphy, T. Calarco, R. Fazio, S. Montangero, V. Giovannetti, and G. E. Santoro, *Phys. Rev. Lett.* **103**, 240501 (2009).
- [14] P. Pyshkin, D.-W. Luo, J. Jing, J. Q. You, and L.-A. Wu, *Sci. Rep.* **6**, 37781 (2016).
- [15] V. Giovannetti, S. Lloyd, and L. Maccone, *Nat. Photon.* **5**, 222 (2011).
- [16] L. Rudnicki, *Phys. Rev. A* **104**, 032417 (2021).
- [17] Z.-Y. Xu, S. Luo, W. L. Yang, C. Liu, and S. Zhu, *Phys. Rev. A* **89**, 012307 (2014).
- [18] Y.-B. Wei, J. Zou, Z.-M. Wang, and B. Shao, *Sci. Rep.* **6**, 1 (2016).
- [19] Z.-R. Zhu, Q. Wang, J. Zou, B. Shao, and L.-A. Wu, *Sci. Rep.* **12**, 1 (2022).

- [20] I. Dzyaloshinsky, *J. Phys. Chem. Solids* **4**, 241 (1958).
- [21] T. J. Siskens, H. Capel, and K. Gaemers, *Physica A* **79**, 259 (1975).
- [22] O. Derzhko, T. Verkholyak, T. Krokhmalkskii, and H. Büttner, *Phys. Rev. B* **73**, 214407 (2006).
- [23] L.-A. Wu, Y.-x. Liu, and F. Nori, *Phys. Rev. A* **80**, 042315 (2009).
- [24] V. Eisler and Z. Zimborás, *Phys. Rev. A* **71**, 042318 (2005).
- [25] T. Antal, Z. Rácz, and L. Sasvári, *Phys. Rev. Lett.* **78**, 167 (1997).
- [26] M. D. Grynberg, T. J. Newman, and R. B. Stinchcombe, *Phys. Rev. E* **50**, 957 (1994).
- [27] P. G. J. van Dongen, *Phys. Rev. B* **49**, 7904 (1994).
- [28] E. Lieb, T. Schultz, and D. Mattis, *Ann. Phys.* **16**, 407 (1961).
- [29] R. Jafari, M. Kargarian, A. Langari, and M. Siahatgar, *Phys. Rev. B* **78**, 214414 (2008).
- [30] T. Krokhmalkskii, O. Derzhko, J. Stolze, and T. Verkholyak, *Phys. Rev. B* **77**, 174404 (2008).
- [31] F.-W. Ma, S.-X. Liu, and X.-M. Kong, *Phys. Rev. A* **84**, 042302 (2011).
- [32] B.-Q. Liu, B. Shao, J.-G. Li, J. Zou, and L.-A. Wu, *Phys. Rev. A* **83**, 052112 (2011).
- [33] M. Azimi, M. Sekania, S. K. Mishra, L. Chotorlishvili, Z. Toklikishvili, and J. Berakdar, *Phys. Rev. B* **94**, 064423 (2016).
- [34] S. Sachdev, *Quantum Phase Transitions* (Cambridge University Press, Cambridge, 2011).
- [35] S. Roy, T. Chanda, T. Das, D. Sadhukhan, A. Sen De, and U. Sen, *Phys. Rev. B* **99**, 064422 (2019).
- [36] K. Cao, Z. Ming, and P. Tong, [arXiv:2106.00191](https://arxiv.org/abs/2106.00191).
- [37] H. T. Quan, Z. Song, X. F. Liu, P. Zanardi, and C. P. Sun, *Phys. Rev. Lett.* **96**, 140604 (2006).
- [38] Z.-G. Yuan, P. Zhang, and S.-S. Li, *Phys. Rev. A* **75**, 012102 (2007).
- [39] R. Jafari and H. Johannesson, *Phys. Rev. B* **96**, 224302 (2017).
- [40] K. Funo, J.-N. Zhang, C. Chatou, K. Kim, M. Ueda, and A. del Campo, *Phys. Rev. Lett.* **118**, 100602 (2017).
- [41] M. Zhong, H. Xu, X.-X. Liu, and P.-Q. Tong, *Chin. Phys. B* **22**, 090313 (2013).
- [42] Q. Wang, Z.-R. Zhu, J. Zou, and B. Shao, *Commun. Theor. Phys.* **74**, 115102 (2022).
- [43] D. P. Pires, M. Cianciaruso, L. C. Céleri, G. Adesso, and D. O. Soares-Pinto, *Phys. Rev. X* **6**, 021031 (2016).
- [44] J. Anandan and Y. Aharonov, *Phys. Rev. Lett.* **65**, 1697 (1990).
- [45] M. Hübner, *Phys. Lett. A* **163**, 239 (1992).
- [46] M. Cianciaruso, S. Maniscalco, and G. Adesso, *Phys. Rev. A* **96**, 012105 (2017).
- [47] A. del Campo, I. L. Egusquiza, M. B. Plenio, and S. F. Huelga, *Phys. Rev. Lett.* **110**, 050403 (2013).